Rapid Whole-Knee Quantification of Cartilage Using T_1, T_2^*, and T_{RAFF2} Mapping With Magnetic Resonance Fingerprinting

Tourais, Joao; Ploem, Telly; Zadelhoff, Tijmen A.van; Steeg-Henzen, Christal van de; Oei, Edwin H.G.; Weingartner, Sebastian

DOI
10.1109/TBME.2023.3280115

Publication date
2023

Document Version
Final published version

Published in
IEEE Transactions on Biomedical Engineering

Rapid Whole-Knee Quantification of Cartilage Using T_1, T_2^*, and T_{RAFF2} Mapping With Magnetic Resonance Fingerprinting

Joao Tourais, Telly Ploem, Tijmen A. van Zadelhoff, Christal van de Steeg-Henzen, Edwin H. G. Oei, and Sebastian Weingärtner

Abstract*—*Objective: **Quantitative Magnetic Resonance Imaging (MRI) holds great promise for the early detection of cartilage deterioration. Here, a Magnetic Resonance Fingerprinting (MRF) framework is proposed for comprehensive and rapid quantification of T_1, T_2^*, and T_{RAFF2} with whole-knee coverage.** ***Methods:*** **A MRF framework was developed to achieve quantification of Relaxation Along a Fictitious Field in the 2nd rotating frame of reference (T_{RAFF2}) along with T_1 and T_2^*. The proposed sequence acquires 65 measurements of 25 high-resolution slices, interleaved with 7 inversion pulses and 40 RAFF2 trains, for whole-knee quantification in a total acquisition time of 3:25 min. Comparison with reference T_1, T_2^*, and T_{RAFF2} methods was performed in phantom and in seven healthy subjects at 3 T. Repeatability (test-retest) with and without repositioning was also assessed.** ***Results:*** **Phantom measurements resulted in good agreement between MRF and the reference with mean biases of -54, 2, and 5 ms for T_1, T_2^*, and T_{RAFF2}, respectively. Complete characterization of the whole-knee cartilage was achieved for all subjects, and, for the femoral and tibial compartments, a good agreement between MRF and reference measurements was obtained. Across all subjects, the proposed MRF method yielded acceptable repeatability without repositioning ($R^2 \geq 0.94$) and with repositioning ($R^2 \geq 0.57$) for T_1, T_2^*, and T_{RAFF2}.** ***Significance:*** **The short scan time combined with the whole-knee coverage makes the proposed MRF framework a promising candidate for the early assessment of cartilage degeneration with quantitative MRI, but further research may be warranted to improve repeatability after repositioning and assess clinical value in patients.**

Manuscript received 1 July 2022; revised 3 February 2023 and 5 May 2023; accepted 12 May 2023. Date of publication 25 May 2023; date of current version 20 October 2023. This work was supported in part by the 4TU federation, a NWO Start-up under Grant STU.019.024 and in part by ZonMW Off-Road 04510011910073. Associate Editor: Dr. Jim Xiuquan Ji. *(Corresponding author: Sebastian Weingärtner.)*

Joao Tourais and Telly Ploem are with the Magnetic Resonance Systems Lab, Department of Imaging Physics, Delft University of Technology, 2628 CD Delft, The Netherlands.

Tijmen A. van Zadelhoff and Edwin H. G. Oei are with the Department of Radiology and Nuclear Medicine, Erasmus University Medical Center Rotterdam, The Netherlands.

Christal van de Steeg-Henzen is with HollandPTC, The Netherlands.

Sebastian Weingärtner is with the Magnetic Resonance Systems Lab, Department of Imaging Physics, Delft University of Technology, 2628 CD Delft, The Netherlands (e-mail: S.Weingartner@tudelft.nl).

This article has supplementary downloadable material available at https://doi.org/10.1109/TBME.2023.3280115, provided by the authors.

Digital Object Identifier 10.1109/TBME.2023.3280115

***Index Terms*—Cartilage, magnetic resonance fingerprinting, quantitative MRI, RAFF mapping, T_1 mapping, T_2^* mapping, whole-knee.**

I. Introduction

EARLY detection of cartilage damage in the knee is essential to prevent or decelerate progressive and/or irreversible joint damage [1]. Noninvasive measurement of quantitative MRI biomarkers allows the detection of functional and nonmorphological changes beyond standard clinical qualitative MRI techniques [2]. Several quantitative biomarkers have shown sensitivity to cartilage degeneration, including, T_1 relaxation times, which demonstrated sensitivity to changes in the proteoglycan content [3] or T_2^* relaxation times, which are sensitive to water content and collagen fiber network changes [4], [5].

Rotating frame of reference (RFR) relaxation measurements, such as $T_{1\rho}$ mapping [6], have shown promising results as a quantitative biomarker due to high sensitivity to slow molecular motion in the cartilage [7]. RFR measurements are most commonly obtained using spin-lock pulses to induce variable $T_{1\rho}$ weighting in a series of images. However, spin-lock pulses are typically long pulses with high amplitudes, and their application at high field strength (3 T and above) is hampered by limits of the specific absorption rate (SAR) [8]. Relaxation along a fictitious field (RAFF) is an alternative RFR contrast, which employs amplitude- and frequency-modulated pulses in the subadiabatic regime to create RFR contrast [9]. Recently, the relaxation time of RAFF in the second rotating frame of reference (T_{RAFF2}) has shown promising results in the detection of cartilage degeneration in different ex vivo species (bovine [10], rabbits [11], [12], piglets [13], and ponies [14]). Compared to $T_{1\rho}$ mapping, at the same peak RF amplitude, RAFF mapping has low SAR requirements with good resilience against B_0 and B_1^+ inhomogeneities [9]. Together, this renders T_{RAFF2} as an extremely promising contrast mechanism and quantitative biomarker, for high-field imaging of the articular cartilage.

Conventional quantitative mapping techniques usually acquire only one single-parameter map per scan by generating multiple, single-parameter weighted images, which are then fitted voxel-wise to the corresponding signal model. However, different relaxometry-based biomarkers provide complementary information about the cartilage state and no single biomarker has

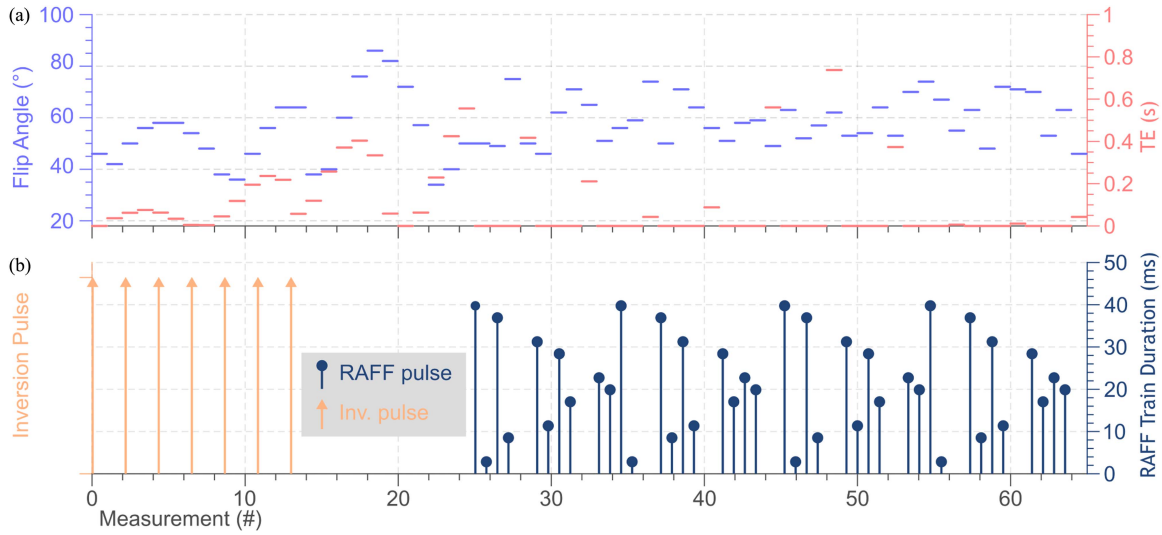

Fig. 1. (a) Flip Angle and Echo Time (TE) are varied for each of the 65 measurements. (b) Seven adiabatic inversion pulses are distributed throughout the sequence for improved T_1 encoding. RAFF contrast was achieved by adding 40 RAFF trains of varying duration throughout the latter part of the sequence.

been accepted as the standard [15]. Therefore, multiparametric quantification bears promise for a more sensitive and specific diagnosis of cartilage degeneration [16]. Independent acquisition of single-parameter maps requires long scan times, and the need to coregister the different maps hampers image fusion. Magnetic resonance fingerprinting (MRF) has been proposed as a promising approach to this problem by varying multiple acquisition parameters such as flip angle (FA), echo time (TE), and repetition time (TR) simultaneously throughout a single acquisition [17]. The resulting signal evolution is subsequently matched to a simulated signal response for the underlying tissue parameters, resulting in inherently co-registered relaxation maps. Recently, MRF has been successfully applied for T_1, T_2, and $T_{1\rho}$ tissue characterization of the human knee articular cartilage in 2D [18] and 3D [19], allowing for differentiation between mild osteoarthritis patients and healthy subjects. MRF was also applied to the human knee for simultaneous estimation of different relaxometry biomarkers (e.g., T_1, T_2) and fat fraction [20], [21], and blood flow velocity maps [22]. MRF based on Cartesian echo-planar imaging (EPI) readout (MRF-EPI) has been introduced, enabling rapid multiparameter mapping and efficient multislice coverage with interpretable and high-SNR baseline images [23], [24].

In this study, we explore the use of MRF-EPI for efficient, simultaneous multiparameter mapping of T_1, T_2^*, and T_{RAFF2} of the whole-knee. A slice interleaved MRF-EPI sequence is extended to measure T_1, T_2^*, and T_{RAFF2} in clinically acceptable scan times. Phantom and in vivo measurements are performed at 3 T to investigate the accuracy and repeatability of the proposed method.

II. Methods

A. Sequence Design

Fig. 1 shows a schematic of the proposed pulse sequence. A slice-interleaved multislice MRF-EPI sequence [24] was extended to incorporate the measurement of T_1, T_2^*, and T_{RAFF2}. Several gradient-echo planar imaging measurements per slice are acquired with varying FA and TE, to encode T_1 and T_2^*. A spectrally selective fat saturation module [25] is applied before each EPI readout excitation, as commonly used to suppress chemical-shift artifacts in EPI-based sequences [26]. Adiabatic inversion pulses are distributed throughout the initial part of the sequence for enhanced T_1 encoding. T_{RAFF2} quantification was achieved by adding RAFF pulse trains throughout the last part of the proposed sequence. The RAFF trains vary in duration and comprise one or more RAFF2 pulses [9] interleaved with short spoiler blips, as shown in Fig. 2.

Image reconstruction was performed inline at the scanner using the vendor's implementation of correction for gradient delay errors, eddy-current induced deviations, and distortion corrections [27]. Dictionary calculation and matching were generated offline using MATLAB (The MathWorks; Natick, MA, USA). The dictionary was simulated using the Bloch equations assuming an isochromatic voxel. Gradient and RF spoiling was assumed to be complete, and simulated by complete loss of the transverse magnetization in the isochromat. Perfect inversion was assumed after the inversion pulses, which were considered to be ideal (180°) with no T_2 decay during the pulse. To compensate for deviations from the nominal flip angle excitation pulse, due to imperfect slice profiles excitation and inhomogeneities in the transmit field, a B_1^+ correction was implemented within the dictionary [23], [28]. Dictionary matching was performed by choosing the entry with the highest inner product between the magnitude of the dictionary entry and the magnitude of the measured signal. RAFF pulses were modeled as a two-parameter monoexponential decay function, $S(t) = A \cdot e^{-\frac{t}{T_{RAFF2}}}$, assuming negligible steady-state magnetization [9] in the dictionary generation. The Levenberg-Marquardt algorithm was used as the optimization method. T_1 times ranged from 100 to 3500 ms, and T_2^* and T_{RAFF2} ranged from 10 to 400 ms, all with 5% increments. Unrealistic entries with $T_1 < T_2^*$ were discarded. FA

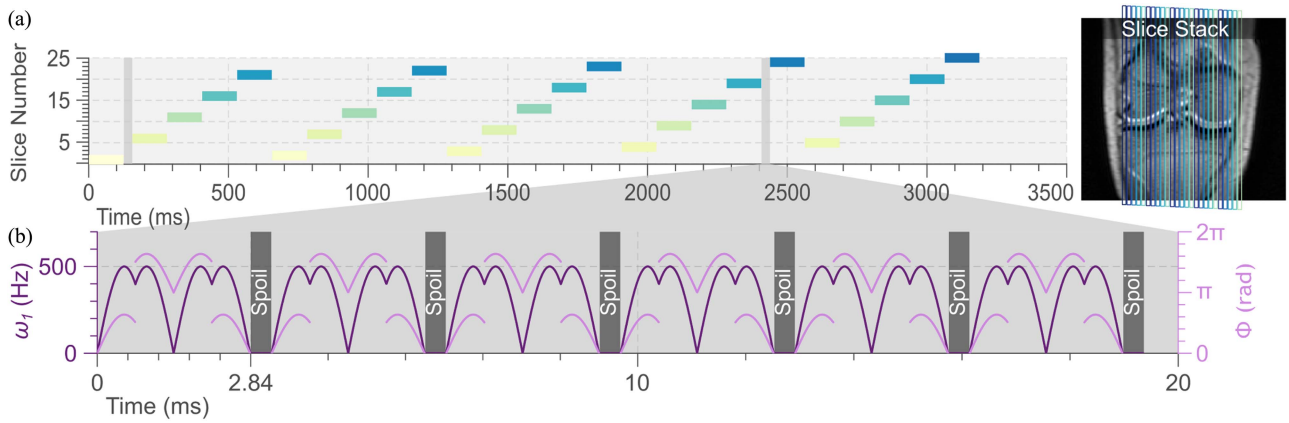

Fig. 2. Schematic of the proposed multislice MRF pulse sequence framework. (a) Whole-knee imaging is performed using a slice-interleaved scheme with 25 slices being acquired for each measurement. Preparation pulses, inversion, or RAFF trains, are placed at different time points of the interleaved slice acquisition (i.e., the slice number immediately following the preparation vary throughout the acquisition). (b) RAFF trains comprise several RAFF pulses separated with spoiler blips. RAFF employs amplitude- (purple) and frequency-modulated (pink) pulses in the subadiabatic regime.

efficiency (B_1^+) ranged from 0.6 to 1.2 with increments of 0.1, resulting in a total dictionary size of 2,765,544 entries. Total time for dictionary generation was 64 min, with the matching taking 7 min for 25 slices. Implementation of the proposed method is provided online (https://gitlab.tudelft.nl/mars-lab/mrf-epi-raff2).

B. MR Imaging

Phantom and in vivo imaging was performed on a 3 T MRI scanner (Ingenia; Philips, Best, The Netherlands) with an 8-channel knee coil.

Phantom measurements, using the T1MES phantom [29], were performed to evaluate the bias and precision of the MRF sequence compared to the reference measurements. To assess repeatability of the proposed MRF method, phantom measurements were acquired once without re-positioning (test - re-test 1) and again after re-positioning (test - re-test 2). Additionally, to assess the performance of the MRF sequence, five different flip angle patterns were used and the measured T_1, T_2^*, and T_{RAFF2} were compared.

The following parameters were kept constant for MRF-EPI and reference maps for both the phantom and in vivo experiments: FOV = 160 mm × 160 mm, matrix size (base resolution) = 200 × 200 (0.8 mm × 0.8 mm), slice thickness = 3 mm. RAFF2 was performed with an RF peak amplitude of 500 Hz (corresponding to 11.74 μT B_1).

In the proposed MRF-EPI sequence, the acquisition parameters were as follow: Number of slices = 25, SENSE = 2.5, partial Fourier = 0.6, variable FA (34–86°), TE (18.0–78.5 ms), TR (109.3–169.8 ms), inversion pulse (pulse duration) = tan-tanh (4.43 ms) [30], number of inversion pulses = 7, RAFF2 trains = 40, RAFF spoiler blip duration = 200 μs. The total scan time was 3:25 min.

For T_1 quantification, a single-slice reference inversion-recovery gradient echo was performed with TI = 50, 100, 200, 400, 800, 1600, 3200 ms, FA = 35°, TE/TR = 2.0/5000 ms, scan time = 5:45 min. A single slice multiple gradient echo was performed for the quantification of the reference T_2^* with 20 different TEs (TE1 = 2.0 ms, ΔTE = 3.2 ms), TR = 600 ms, scan time = 1:14 min. Single-slice reference maps T_{RAFF2} were acquired using a RAFF2-prepared gradient-echo sequence with RAFF2 train duration of 2, 4, 6, 8, 10, 12, FA = 35°, TE/TR = 2.0/5000 ms, scan time = 4:55 min. Reference T_1 maps were computed offline in MATLAB using qMRLab [31] by applying a three-parameter inversion recovery model, $S(t) = A + B \cdot e^{-\frac{t}{T_1}}$ [32]. Reference T_2^* maps were computed inline at the scanner using a two-parameter mono-exponential decay model, $S(t) = A \cdot e^{-\frac{t}{T_2^*}}$. Reference T_{RAFF2} maps were computed offline in MATLAB using qMRLab [31] by applying a two-parameter mono-exponential decay model, $S(t) = A \cdot e^{-\frac{t}{T_{RAFF2}}}$. Implementation of the proposed method is provided online (https://gitlab.tudelft.nl/mars-lab/mrf-epi-raff2)

In vivo imaging was performed in 7 healthy subjects (5 female, 2 male, 29 ± 11 years, range: 19–52 years). The study was performed in accordance with the ethical principles of the Declaration of Helsinki. Ethical approval was obtained from the local research ethics committee. All subjects were informed of the study and provided written informed consent prior to the examination. Multislice MRF and single-slice reference maps were acquired in sagittal orientation, using the same imaging parameters as the phantom experiments. To assess the accuracy of the MRF technique, the areas of the tibial and femoral cartilage were manually segmented, based on landmarks, using MATLAB on single-slice reference scans and on the corresponding MRF slice. Mean T_1, T_2^*, and T_{RAFF2} of the cartilage segments were calculated. To assess repeatability, the MRF sequence was repeated twice, without repositioning (test - re-test 1). To measure intra-subject repeatability with repositioning, additional test/re-test MRF measurements were performed (test - re-test 2), where the subject was asked to exit the scanner bore, and a new set of MRF images was acquired after repositioning [33]. The three central slices for each medial and lateral compartments were

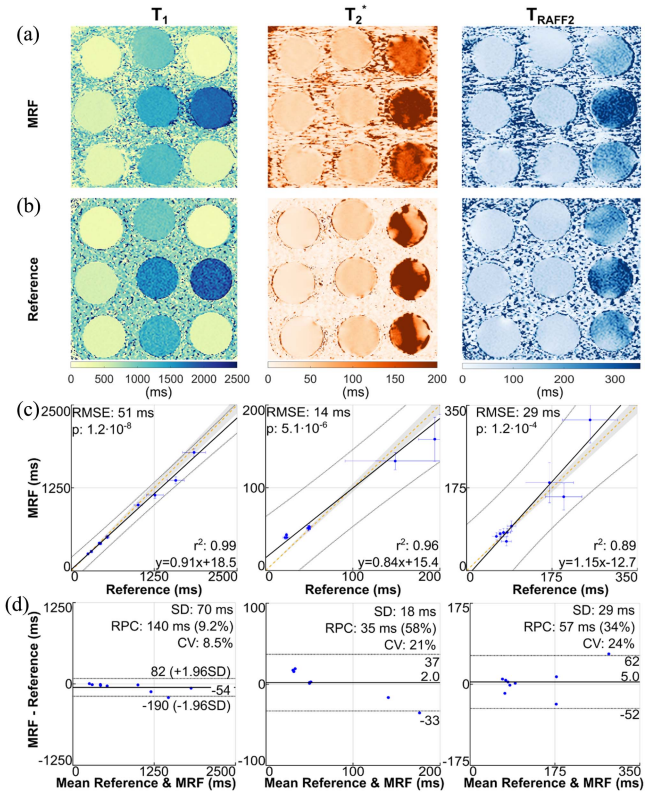

Fig. 3. Comparison of T_1, T_2^*, and T_{RAFF2} obtained with (a) the proposed MRF sequence and (b) the reference protocols. (c) Excellent correlation, between MRF and the reference protocols, was achieved for T_1, T_2^*, and T_{RAFF2} in the phantom experiments. The black lines represent the best linear fit and the gray shading indicates a 5% deviation from the reference (yellow dashed lines). Coefficients of determination (r^2) and best fits are shown for each individual plot. (d) Corresponding Bland-Altman plots. Solid black lines represent mean bias, and dashed black lines represent the limits of agreement ($\pm$1.96 SD). The inset shows the standard deviation (SD), the reproducibility coefficient (RPC) and the Coefficient of Variation (CV).

manually selected for all scans. Central slices were defined as the slice for which the femoral cartilage reached its most inferior position. Subsequently, manual segmentation of the femoral and tibial cartilage areas was performed in those six slices. Across all subjects, correlation and Bland-Altman (BA) analysis were performed for T_1, T_2^*, and T_{RAFF2}.

III. Results

Fig. 3 shows a representative slice using the proposed MRF method and the reference methods, as well as the correlation analysis and the respective Bland-Altman plots of the three relaxation times in the nine vials. T_1, T_2^*, and T_{RAFF2} measured with the proposed MRF-EPI sequence were in excellent agreement with the reference protocols with $R^2 = 0.99$, 0.96, and 0.89, respectively. A bias of -54, 2, and 5 ms was observed for T_1, T_2^*, and T_{RAFF2}, respectively. Excellent repeatability with and without re-positioning was observed for T_1, T_2^*, and T_{RAFF2} in phantom (Fig. S1). Comparable T_1, T_2^*, and T_{RAFF2} was measured with five different flip angle patterns, as shown in Fig. S2.

Data acquisition was successfully performed for all the subjects, below the SAR limits for in vivo scans and no re-shimming was necessary. Fig. S3 shows example baseline images acquired with the proposed MRF method along with representative fingerprints in cartilage ROIs. Fig. 4 shows T_1, T_2^*, and T_{RAFF2} maps of the 25 acquired slices, for a representative subject, providing whole-knee characterization with medial to lateral coverage. The T_1 and T_2^* maps depict largely homogeneous signal in the cartilage. T_{RAFF2} maps exhibited a higher level of signal variation in the cartilage and residual susceptibility to image artifacts.

Fig. 5(a) shows representative slices of T_1, T_2^*, and T_{RAFF2} maps acquired with the proposed MRF-EPI sequence and the reference protocols in two healthy subjects. A clear depiction of the cartilage was achieved, visually distinct from the bone area, on both the MRF and the reference maps. The MRF maps presented a higher level of image distortion, when compared to the reference maps, due to the EPI readout. Fig. 5(b) shows a comparison between the mean femoral and tibial values measured with the MRF and the reference protocols for the seven subjects. Across all subjects, the average $T_1 \pm$ SD values were 1010.5 ± 104.5 ms (femoral) and 1002.3 ± 157.9 ms (tibial) for MRF and 1128.7 ± 107.8 ms (femoral) and 1185.2 ± 133.5 ms (tibial) for the reference maps. T_2^* values were 29.6 ± 3.4 ms (femoral) and 24.8 ± 4.0 ms (tibial) for MRF and 27.1 ± 3.7 ms (femoral) and 20.0 ± 8.6 ms (tibial) for the reference maps. T_{RAFF2} values were 36.7 ± 9.6 ms (femoral) and 38.5 ± 8.5 ms (tibial) for the MRF and 45.2 ± 11.3 ms (femoral) and 51.0 ± 16.9 ms (femoral) for the reference maps. The bias of the measured T_1, T_2^*, and T_{RAFF2} with the proposed MRF-EPI sequence and the reference protocols were -166, 4, and -8 ms, respectively, which were in line with the phantom results. For each subject, the average ($\pm$ SD) T_1, T_2^*, and T_{RAFF2}, as well as the respective Coefficient of Variation (CoV) of the femoral and tibial regions are shown in Fig. S4 measured with MRF and the reference methods. The variability within the cartilage of single subjects is comparable between MRF and the reference methods.

The results of the repeatability with and without repositioning studies are shown in Fig. 6. Across all subjects, excellent intra-subject repeatability was achieved with the proposed MRF-EPI. Between test - re-test 1 measurements, T_1, T_2^*, and T_{RAFF2} achieved very high correlation coefficients ($R^2 = 0.94$, 0.96, and 0.98, respectively) and minimal bias (8.9, -0.3, and 0.2 ms, respectively). Intra-subject repeatability with repositioning experiments also exhibited negligible bias (-2.3, 0.3, and -2.2 ms for T_1, T_2^*, and T_{RAFF2}, respectively), but decreased correlation coefficients were observed between the test - re-test 2 measurements ($R^2 = 0.57$, 0.67, and 0.67, respectively).

IV. Discussion

In this work, whole-knee quantification of T_1, T_2^*, and T_{RAFF2} in the articular cartilage was achieved in less than four minutes. In phantom, the proposed MRF-EPI sequence achieved high accuracy with respect to the reference methods. In healthy subjects, a satisfactory level of intra-subject repeatability with and without repositioning was obtained. This is in line with

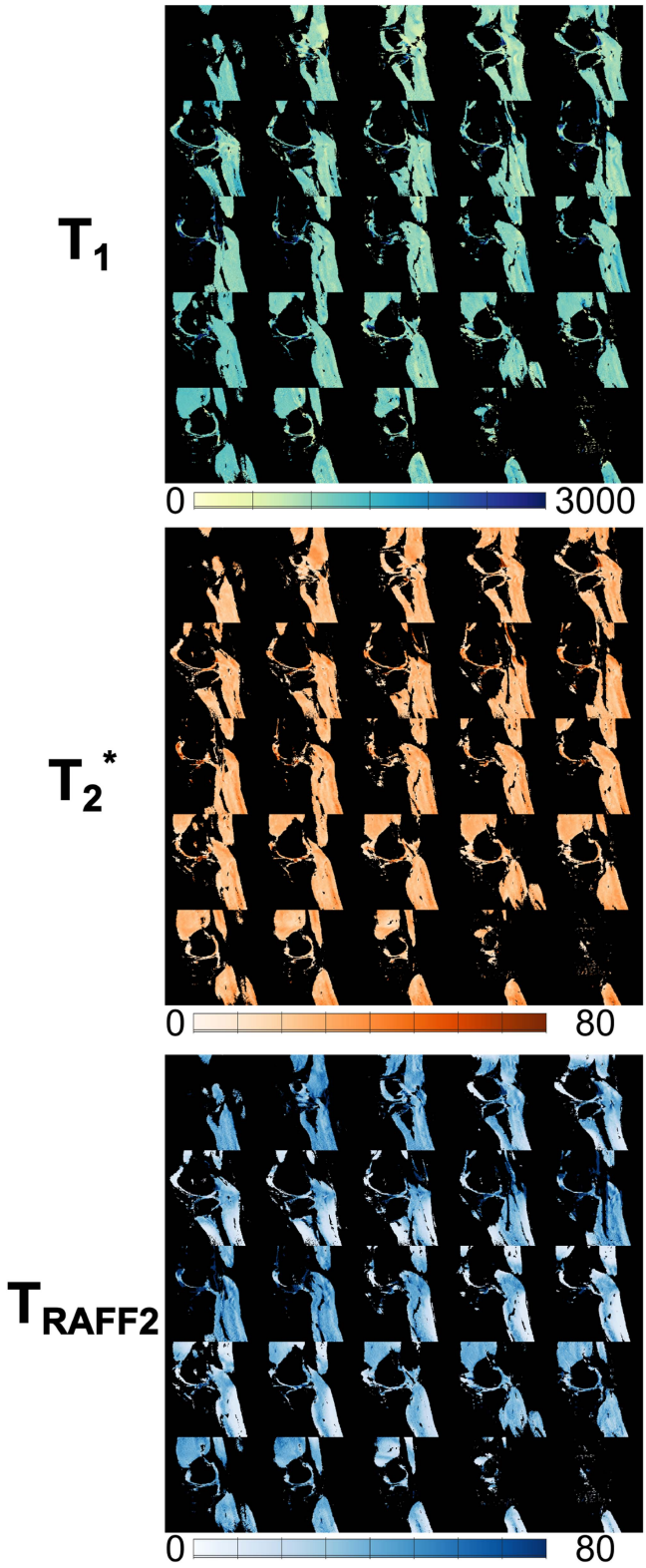

Fig. 4. Simultaneous T_1, T_2^*, and T_{RAFF2} maps for all 25 slices acquired in a healthy subject. The in-plane resolution was 0.8 mm $\times$ 0.8 mm and the total scan time was 3 minutes and 25 seconds. The T_1 and T_2^* maps depict homogeneous signal in the cartilage. T_{RAFF2} maps exhibited a higher level of signal variation in the cartilage and residual susceptibility to image artifacts.

previous MRF-EPI studies in the brain [24] and the kidneys [34] where accurate, whole organ, multiparametric mapping of T_1 and T_2^* was obtained.

In the recent literature, a wide range of T_1 values of knee cartilage measured at 3 T have been reported. Mittal et al. [3] measured an average femoral and tibial T_1 of 912.5 $\pm$ 10.8 ms and 902.3 $\pm$ 22.0 ms, respectively, whereas Sharafi et al. [18] reported a global average T_1 of 778.3 $\pm$ 48.5 ms in healthy tissue. Our T_1 quantification yields slightly higher values compared to the literature and also shows a slight underestimation with respect to the reference methods, in phantom and in vivo. This underestimation can likely be attributed to imperfect inversion efficiency, as the proposed MRF sequence relies on multiple inversions to enhance the sensitivity to T_1. To increase the robustness to B_0 and B_1^+, an adiabatic full passage pulse with relatively long pulse duration was used. During the pulse a nonnegligible amount of relaxation is incurred, which reduces the inversion efficiency [30]. This can potentially be alleviated by alternative inversion pulses, or by taking the magnetization relaxation during the adiabatic inversion pulse into account. However, this would require a more complex dictionary and a larger number of fit variables at the cost of longer computation times and loss in precision. In this work, seven inversion pulses were used, as a trade-off between T_1 precision and scan-time efficiency gains, afforded by acquiring four interleaved slices after a single global inversion pulse, as previously shown [24]. This number of pulses will impact the precision of the measured T_1, and might not be the optimal value for different regions-of-interest. Moreover, in this work, MRF maps were obtained from water-only baseline images due to the use of fat suppression. This may lead to different quantification results than, for example, inversion recovery-based methods, which generate images that include both fat and water signals. Further investigation of clinical sensitivity using water-only maps is warranted in the relevant patient cohorts. Additionally, distortion correction may lead to blurring of the point spread function. However, since it applies to all baseline images, it is not expected to impart bias.

The mean values of the femoral and tibial cartilage T_2^* obtained with the proposed MRF-EPI sequence were in good agreement with previously reported values for 3 T MRI by Hesper et al. (29.8 $\pm$ 5.0 ms) [35] and Zhang et al. (26.4 $\pm$ 2.6 ms and 21.8 $\pm$ 1.8 ms for the femoral and tibial regions, respectively) [5]. Moreover, in this work, a negligible bias was observed for T_2^* obtained with MRF-EPI and a gradient echo reference sequence. Additionally, the fitting procedures used to estimate relaxation time constants assumed that the signal followed a mono-exponential curve. However, recent research suggests that more complex curves, such as multi-exponential functions, may be necessary to accurately model both longitudinal [36], transverse [37], [38], [39] or rotating-frame [40], [41], [42] magnetization behaviors, which can take into account factors like partial volume effects, flow effects, magnetization transfer, and chemical exchange [43], [44]. Further research is warranted to investigate the promise of combining recently emerging multi-component or multi-exponential MRF techniques with the proposed framework [45].

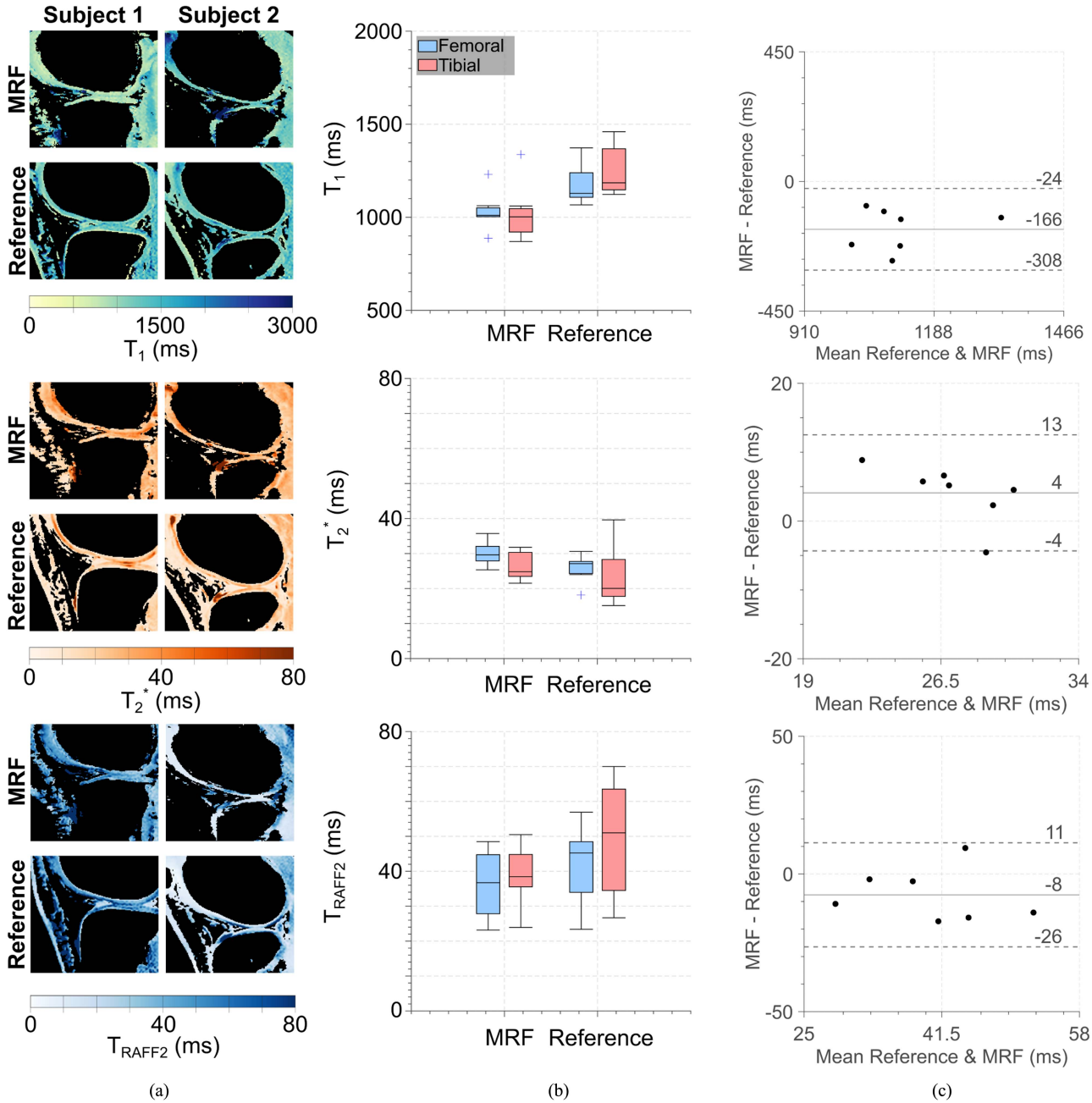

Fig. 5. (a) In vivo T_1, T_2^*, and T_{RAFF2} maps for one slice of MRF and reference scans, for two healthy subjects. (b) Boxplots showing mean femoral and tibial T_1, T_2^*, and T_{RAFF2} across all subjects using the proposed MRF-EPI and the reference methods. In each boxplot, the horizontal line depicts the median, the top and bottom of the box represent the upper and lower quartiles, whereas the whiskers indicate the minimum and maximum values excluding outliers. Additional outliers are indicated by (+). (c) Bland-Altman plot for T_1, T_2^*, and T_{RAFF2} for all subjects.

T_{RAFF2} times have not previously been obtained for articular cartilage in vivo, but the quantification with the proposed MRF-EPI method shows only negligible bias compared to a RAFF2-prepared reference method. T_{RAFF2} maps exhibited a higher level of signal variation and a residual susceptibility to image artifacts compared to the other parameters. However, as RAFF2 operates in a subadiabatic regime, increased RF power may be used to improve resilience of the preparation modules against system imperfections. In the present study the RF peak amplitude was limited to 500 Hz, due to the use of the body coil transmitter. Other scanners or custom transceiver knee coils allow for higher RF power amplitude, and are promising for further improvements in RAFF mapping quality.

MRF maps achieved a substantial reduction in scan time compared to single-slice methods. MRF simultaneously provided T_1, T_2^*, and T_{RAFF2} maps in ≈8 seconds per slice, in contrast to the reference maps, which took ≈345, 74, 295 seconds per slice for T_1, T_2^*, and T_{RAFF2}, respectively. The time efficiency of the proposed sequence makes it a suitable candidate for quantitative rotating frame of reference (RFR) imaging of the knee joint

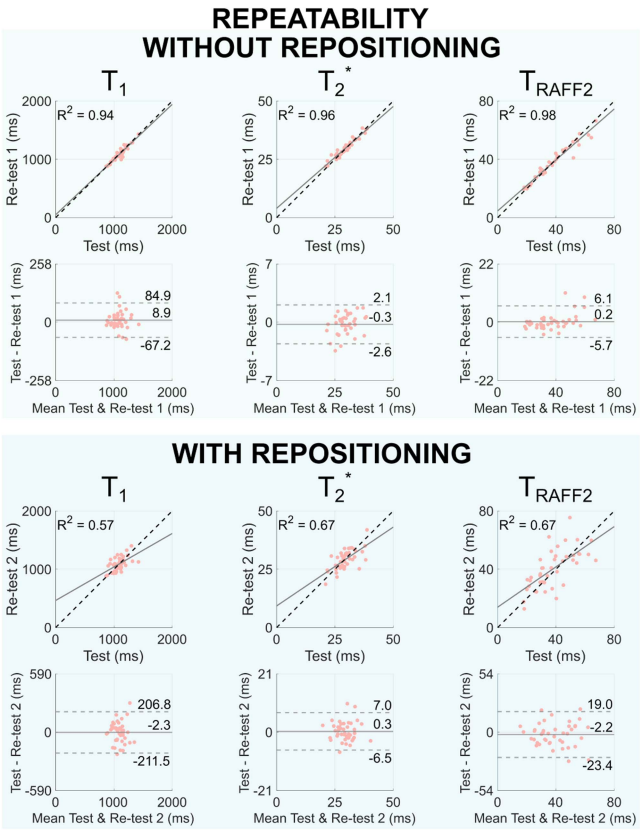

Fig. 6. Correlation and Bland-Altman plots for T_1, T_2^*, and T_{RAFF2} for assessing repeatability without repositioning (top panel) and with repositioning (bottom panel) across all subjects. T_1, T_2^*, and T_{RAFF2} achieved a high correlation factor ($R^2 = 0.94$, 0.96, and 0.98, respectively) and minimal bias (8.9, -0.3, and 0.2 ms, respectively) between measurements without repositioning (test - re-test 1). Negligible bias (-2.3, 0.3, and -2.2 ms for T_1, T_2^*, and T_{RAFF2}, respectively) and moderate correlation factor ($R^2 = 0.57$, 0.67, and 0.67, respectively) were observed for the repeatability experiments before and after repositioning (test - re-test 2).

with or without load in the clinic, which can provide valuable information about joint characteristics [46], [47], [48]. Recently, multislice RFR based on $T_{1\rho}$ mapping quantification has been explored, including 3D-MAPPS [49] and MRF-$T_{1\rho}$ [18], [50]. In comparison, the interleaved slice design with integrated T_1 modeling in the MRF-EPI framework allows for a substantially lower number of preparation pulses per slice. The proposed MRF-EPI sequence uses 40 RFR-prep pulses distributed over 25 slices (< 2 preparations per slice) compared with ≈ 16 preparations per slice (3D-MAPPS) and 6 and 5 preparations (MRF-$T_{1\rho}$), which used a linear ordering for slice acquisition. This approach further reduced the SAR burden and allowed for time-efficient scanning even with SAR heavy-preparation pulses. The multislice acquisition was performed with slice order to maximize the time between the acquisition of adjacent slices. Dictionaries were calculated independently for each slice, assuming minimal slice cross-talk. A simulation of the exact slice profile, and joint matching of all slices, can be explored to further reduce bias due to the slice profile and residual slice cross-talk. However, this comes at the expense of greatly increased reconstruction times, and further research is warranted to make these reconstructions feasible.

The slice-interleaved scheme of the proposed approach allows for highly efficient multi-parametric quantification of the whole knee. However, the total scan time (3:25 min) is longer than single-slice or single-parameter mapping methods, which can be obtained in under 2 minutes (e.g., T_1 [51], T_2^* [52], or T_2 [53]). This increases the risk of motion during the acquisition with the proposed approach. To prevent image quality degradation and maintain diagnostic value, prospective and/or retrospective motion correction can be employed [54], [55], [56]. Shorter scan times can also be achieved by employing advanced acceleration methods, such as simultaneous multislice (SMS) imaging [57], compressed sensing [58], or deep-learning-based reconstructions [59], [60], as previously proposed for cartilage imaging. Furthermore, the fast image readout provided by single-shot EPI is critical for the scan time efficiency. Despite its emerging use in quantitative cartilage imaging [53], [61], [62], [63], [64], [65], EPI-based sequences can be subject to image quality degradation from various sources, such as B_0 inhomogeneities [66], eddy currents, gradient delay errors [67], or susceptibility artifacts [68]. This can result in image distortion [69], [70], [71], blurring, signal loss [72], and Nyquist ghosting artifacts [73], [74], [75], [76], as partly also apparent in some of the phantom and in vivo data (Fig. 3(a) and 5(a), respectively). To improve the resilience of the proposed technique, bipolar EPI imaging with autocalibration [27] and/or the acquisition of field maps [69] can be employed. Additionally, alternative approaches such as multi-shot EPI [77], image regularization [78], or 3D EPI imaging [79], [80] will be explored in future research.

This study has several limitations. In this work, only healthy subjects were scanned to study the feasibility of the proposed MRF-EPI sequence. Future work should be performed to validate the use of the proposed pulse sequence for the early assessment of cartilage degeneration in a cohort of patients with different pathologies. Moreover, further investigation needs to be performed to minimize the negative effect of re-positioning in terms of the repeatability of the proposed method. Furthermore, high-order RAFFn ($n > 2$) [81] could provide further SAR reductions, which could be desired for different anatomies or different field strengths. Additionally, to improve the image quality of the computed maps with the proposed MRF sequence, filtering [34] could be applied to the baseline images to minimize the effect of EPI k-space sampling. Also, the SNR of the parametric maps could be further improved by optimizing the FA/TE train of the pulse sequence for the range of T_1 and T_2^* values expected in the knee cartilage. No image registration was performed between MRF and reference maps. In this study, Gaussian noise is implicitly assumed, as the inner product was used as the loss function in dictionary matching. However, when the SNR is too low, the Rician noise distribution increasingly deviates from Gaussianity, which can lead to bias in the measurements. This can be mitigated by using phase-sensitive reconstructions, which are specifically designed to handle Rician noise, particularly if no partial Fourier is used. Finally, in the reference methods, conventional Cartesian k-space sampling was employed instead of EPI, to obtain the highest image quality.

V. Conclusion

In this study, T_1, T_2^*, and T_{RAFF2} mapping of the whole-knee articular cartilage was achieved in just under four minutes. An MRF-EPI sequence was extended to include T_{RAFF2} resulting in inherently co-registered high-quality maps, with good visual map quality and with clinically tolerable specific absorption rates (SAR). The proposed method also achieved good levels of repeatability with and without repositioning in phantom and in vivo. The short scan time combined with the quantification of the whole-knee makes the proposed MRF-EPI sequence an excellent candidate for the early assessment of cartilage degeneration, but further research may be warranted to improve repeatability with repositioning and assess clinical value in patients.

References

[1] S. Brinkhof et al., "T2* mapping in an equine articular groove model: Visualizing changes in collagen orientation," *J. Orthop. Res.*, vol. 38, no. 11, pp. 2383–2389, 2020.

[2] S. J. Matzat et al., "Quantitative MRI techniques of cartilage composition," *Quantitative Imag. Med. Surg.*, vol. 3, no. 3, pp. 162–174, 2013.

[3] S. Mittal et al., "T1 and T2 mapping of articular cartilage and menisci in early osteoarthritis of the knee using 3-tesla magnetic resonance imaging," *Polish J. Radiol.*, vol. 84, pp. e549–e564, 2019.

[4] T. Hesper et al., "T2* mapping for articular cartilage assessment: Principles, current applications, and future prospects," *Skeletal Radiol*, vol. 43, no. 10, pp. 1429–1445, 2014.

[5] P. Zhang et al., "Longitudinal study of the morphological and T2* changes of knee cartilages of marathon runners using prototype software for automatic cartilage segmentation," *Brit. J. Radiol.*, vol. 94, no. 1119, 2021, Art. no. 20200833.

[6] A. Borthakur et al., "Sodium and T1RHO MRI for molecular and diagnostic imaging of articular cartilage," *NMR Biomed.*, vol. 19, no. 7, pp. 781–821, 2006.

[7] Y. Xia, "MRI of articular cartilage at microscopic resolution," *Bone Joint Res.*, vol. 2, no. 1, pp. 9–17, 2013.

[8] A. Borthakur et al., "Three-dimensional t1rho-weighted MRI at 1.5 tesla," *J. Magn. Reson. Imag.*, vol. 17, no. 6, pp. 730–736, 2003.

[9] T. Liimatainen et al., "MRI contrast from relaxation along a fictitious field (RAFF)," *Magn. Reson. Med.*, vol. 64, no. 4, pp. 983–994, 2010.

[10] J. Ellermann et al., "MRI rotating frame relaxation measurements for articular cartilage assessment," *Magn. Reson. Imag.*, vol. 31, no. 9, pp. 1537–1543, 2013.

[11] J. Rautiainen et al., "Adiabatic rotating frame relaxation of MRI reveals early cartilage degeneration in a rabbit model of anterior cruciate ligament transection," *Osteoarthritis Cartilage*, vol. 22, no. 10, pp. 1444–1452, 2014.

[12] A. W. Kajabi et al., "Multiparametric MR imaging reveals early cartilage degeneration at 2 and 8 weeks after ACL transection in a rabbit model," *J. Orthop. Res.*, vol. 38, no. 9, pp. 1974–1986, 2020.

[13] C. P. Johnson et al., "Quantitative MRI helps to detect hip ischemia: Preclinical model of legg-calve-perthes disease," *Radiol.*, vol. 289, no. 2, pp. 386–395, 2018.

[14] A. W. Kajabi et al., "Evaluation of articular cartilage with quantitative MRI in an equine model of post-traumatic osteoarthritis," *J. Orthop. Res.*, vol. 39, no. 1, pp. 63–73, 2021.

[15] E. Y. Chang, Y. Ma, and J. Du, "MR parametric mapping as a biomarker of early joint degeneration," *Sports Health*, vol. 8, no. 5, pp. 405–411, 2016.

[16] J. Thuring et al., "Multiparametric MRI and computational modelling in the assessment of human articular cartilage properties: A comprehensive approach," *Biomed. Res. Int.*, vol. 2018, p. 12, 2018, Art. no. 9460456, doi: 10.1155/2018/9460456.

[17] D. Ma et al., "Magnetic resonance fingerprinting," *Nature*, vol. 495, no. 7440, pp. 187–192, 2013.

[18] A. Sharafi et al., "MR fingerprinting for rapid simultaneous T1, T2, and T1 rho relaxation mapping of the human articular cartilage at 3T," *Magn. Reson. Med.*, vol. 84, no. 5, pp. 2636–2644, 2020.

[19] A. Sharafi et al., "3D magnetic resonance fingerprinting for rapid simultaneous T1, T2, and T1RHO volumetric mapping of human articular cartilage at 3T," *NMR Biomed.*, vol. 35, no. 12, 2022, Art. no. e4800.

[20] M. Cencini et al., "Magnetic resonance fingerprinting with dictionary-based fat and water separation (DBFW MRF): A multi-component approach," *Magn. Reson. Med.*, vol. 81, no. 5, pp. 3032–3045, 2019.

[21] J. Ostenson, B. M. Damon, and E. B. Welch, "MR fingerprinting with simultaneous T1, T2, and fat signal fraction estimation with integrated b0 correction reduces bias in water T1 and T2 estimates," *Magn. Reson. Imag.*, vol. 60, pp. 7–19, 2019.

[22] S. Flassbeck et al., "Flow MR fingerprinting," *Magn. Reson. Med.*, vol. 81, no. 4, pp. 2536–2550, 2019.

[23] B. Rieger et al., "Magnetic resonance fingerprinting using echo-planar imaging: Joint quantification of T1 and T2 * relaxation times," *Magn. Reson. Med.*, vol. 78, no. 5, pp. 1724–1733, 2017.

[24] B. Rieger et al., "Time efficient whole-brain coverage with MR fingerprinting using slice-interleaved echo-planar-imaging," *Sci. Rep.*, vol. 8, no. 1, 2018, Art. no. 6667.

[25] A. Haase et al., "1H NMR chemical shift selective (CHESS) imaging," *Phys. Med. Biol.*, vol. 30, no. 4, pp. 341–344, 1985.

[26] R. R. Edelman, P. Wielopolski, and F. Schmitt, "Echo-planar MR imaging," *Radiol.*, vol. 192, no. 3, pp. 600–612, 1994.

[27] V. J. Schmithorst, B. J. Dardzinski, and S. K. Holland, "Simultaneous correction of ghost and geometric distortion artifacts in EPI using a multi-echo reference scan," *IEEE Trans. Med. Imag.*, vol. 20, no. 6, pp. 535–539, Jun. 2001.

[28] G. Buonincontri and S. J. Sawiak, "MR fingerprinting with simultaneous B1 estimation," *Magn. Reson. Med.*, vol. 76, no. 4, pp. 1127–1135, 2016.

[29] G. Captur et al., "A medical device-grade T1 and ECV phantom for global T1 mapping quality assurance-the T1 mapping and ECV standardization in cardiovascular magnetic resonance (T1MES) program," *J. Cardiovasc Magn. Reson.*, vol. 18, no. 1, pp. 1–20, 2016.

[30] P. Kellman, D. A. Herzka, and M. S. Hansen, "Adiabatic inversion pulses for myocardial T1 mapping," *Magn. Reson. Med.*, vol. 71, no. 4, pp. 1428–1434, 2014.

[31] A. Karakuzu et al., "QMRLAB: Quantitative MRI analysis, under one umbrella," *J. Open Source Softw.*, vol. 5, no. 53, 2020, Art. no. 2343.

[32] J. K. Barral et al., "A robust methodology for in vivo T1 mapping," *Magn. Reson. Med.*, vol. 64, no. 4, pp. 1057–1067, 2010.

[33] S. Weingartner et al., "Development, validation, qualification, and dissemination of quantitative MR methods: Overview and recommendations by the ISMRM quantitative mr study group," *Magn. Reson. Med.*, vol. 87, no. 3, pp. 1184–1206, 2022.

[34] I. Hermann et al., "Magnetic resonance fingerprinting for simultaneous renal T1 and T 2 * mapping in a single breath-hold," *Magn. Reson. Med.*, vol. 83, no. 6, pp. 1940–1948, 2020.

[35] T. Hesper et al., "Quantitative T2(*) assessment of knee joint cartilage after running a marathon," *Eur. J. Radiol.*, vol. 84, no. 2, pp. 284–289, 2015.

[36] C. Labadie et al., "Myelin water mapping by spatially regularized longitudinal relaxographic imaging at high magnetic fields," *Magn. Reson. Med.*, vol. 71, no. 1, pp. 375–387, 2014.

[37] S. Wharton and R. Bowtell, "Fiber orientation-dependent white matter contrast in gradient echo MRI," *Proc. Nat. Acad. Sci.*, vol. 109, no. 45, pp. 18559–18564, 2012.

[38] D. Hwang, D. H. Kim, and Y. P. Du, "In vivo multi-slice mapping of myelin water content using T2* decay," *Neuroimage*, vol. 52, no. 1, pp. 198–204, 2010.

[39] P. van Gelderen et al., "Nonexponential T(2) decay in white matter," *Magn. Reson. Med.*, vol. 67, no. 1, pp. 110–117, 2012.

[40] V P. Mlynárik et al., "Transverse relaxation mechanisms in articular cartilage," *J. Magn. Reson.*, vol. 169, no. 2, pp. 300–307, 2004.

[41] A. Sharafi et al., "Biexponential T1 relaxation mapping of human knee cartilage in vivo at 3T," *NMR Biomed.*, vol. 30, no. 10, 2017, Art. no. e3760.

[42] A. Sharafi, G. Chang, and R. R. Regatte, "Bi-component T1 and T2 relaxation mapping of skeletal muscle in-vivo," *Sci. Rep.*, vol. 7, 2017, Art. no 14115.

[43] G. J. Stanisz and R. M. Henkelman, "Gd-DTPA relaxivity depends on macromolecular content," *Magn. Reson. Med.*, vol. 44, no. 5, pp. 665–667, 2000.

[44] A. N. Dula et al., "Multiexponential T2, magnetization transfer, and quantitative histology in white matter tracts of rat spinal cord," *Magn. Reson. Med.*, vol. 63, no. 4, pp. 902–909, 2010.

[45] M. Nagtegaal et al., "Fast multi-component analysis using a joint sparsity constraint for MR fingerprinting," *Magn. Reson. Med.*, vol. 83, no. 2, pp. 521–534, 2020.

[46] D. Nag et al., "Quantification of T(2) relaxation changes in articular cartilage with in situ mechanical loading of the knee," *J. Magn. Reson. Imag.*, vol. 19, no. 3, pp. 317–322, 2004.

[47] H. Hamada et al., "Comparison of load responsiveness of cartilage T1rho and T2 in porcine knee joints: An experimental loading MRI study," *Osteoarthritis Cartilage*, vol. 23, no. 10, pp. 1776–1779, 2015.
[48] J. Boon et al., "Magnetic resonance imaging compatible elastic loading mechanism (MELM): A minimal footprint device for MR imaging under load," in *Proc. IEEE 43rd Annu. Int. Conf. Eng. Med. Biol. Soc.*, 2021, pp. 3721–3724.
[49] X. Li et al., "In vivo t(1rho) mapping in cartilage using 3D magnetization-prepared angle-modulated partitioned k-space spoiled gradient echo snapshots (3D MAPSS)," *Magn. Reson. Med.*, vol. 59, no. 2, pp. 298–307, 2008.
[50] C. R. Wyatt, T. M. Barbara, and A. R. Guimaraes, "T1rho magnetic resonance fingerprinting," *NMR Biomed.*, vol. 33, no. 5, 2020, Art. no. e4284.
[51] G. Cao, S. Gao, and B. Xiong, "Application of quantitative T1, T2 and T2* mapping magnetic resonance imaging in cartilage degeneration of the shoulder joint," *Sci Rep*, vol. 13, no. 1, 2023, Art. no. 4558.
[52] G. H. Welsch et al., "T2 and T2* mapping in patients after matrix-associated autologous chondrocyte transplantation: Initial results on clinical use with 3. 0-tesla MRI," *Eur. Radiol*, vol. 20, no. 6, pp. 1515–1523, 2010.
[53] E. Quaia et al., "Fast T2 mapping of the patellar articular cartilage with gradient and spin-echo magnetic resonance imaging at 1.5 t: Validation and initial clinical experience in patients with osteoarthritis," *Skeletal Radiol.*, vol. 37, no. 6, pp. 511–517, 2008.
[54] T. Lange et al., "Comparative T2 and T1rho mapping of patellofemoral cartilage under in situ mechanical loading with prospective motion correction," *J. Magn. Reson. Imag.*, vol. 46, no. 2, pp. 452–460, 2017.
[55] Z. Dong et al., "Motion-corrected k-space reconstruction for interleaved EPI diffusion imaging," *Magn. Reson. Med.*, vol. 79, no. 4, pp. 1992–2002, 2018.
[56] G. Cruz et al., "Rigid motion-corrected magnetic resonance fingerprinting," *Magn. Reson. Med.*, vol. 81, no. 2, pp. 947–961, 2019.
[57] M. Barth et al., "Simultaneous multislice (SMS) imaging techniques," *Magn. Reson. Med.*, vol. 75, no. 1, pp. 63–81, 2016.
[58] M. V. W. Zibetti et al., "Rapid compositional mapping of knee cartilage with compressed sensing MRI," *J. Magn. Reson. Imag.*, vol. 48, no. 5, pp. 1185–1198, 2018.
[59] Y. Wu et al., "Incorporating prior knowledge via volumetric deep residual network to optimize the reconstruction of sparsely sampled MRI," *Magn. Reson. Imag.*, vol. 66, pp. 93–103, 2020.
[60] N. Subhas et al., "Diagnostic interchangeability of deep convolutional neural networks reconstructed knee MR images: Preliminary experience," *Quantitative Imag. Med. Surg.*, vol. 10, no. 9, pp. 1748–1762, 2020.
[61] A. H. Karantanas, A. H. Zibis, and N. Papanikolaou, "Comparison of echo planar imaging, gradient echo and fast spin echo MR scans of knee menisci," *Comput. Med. Imag. Graph.*, vol. 24, no. 5, pp. 309–316, 2000.
[62] A. Ba-Ssalamah et al., "Imaging articular cartilage defects in the ankle joint with 3D fat-suppressed echo planar imaging: Comparison with conventional 3D fat-suppressed gradient echo imaging," *J. Magn. Reson. Imag.*, vol. 16, no. 2, pp. 209–216, 2002.
[63] A. H. Karantanas, A. H. Zibis, and P. Kitsoulis, "Fat-suppressed 3D-T1-weighted-echo planar imaging: Comparison with fat-suppressed 3D-T1-weighted-gradient echo in imaging the cartilage of the knee," *Comput. Med. Imag. Graph.*, vol. 26, no. 3, pp. 159–165, 2002.
[64] S. C. Zhu, D. P. Shi, and A. Xuan, "Human patellar cartilage: Echo planar diffusion-weighted MR imaging findings at 3.0 t," *Clin. Imag.*, vol. 36, no. 3, pp. 199–202, 2012.
[65] T. Ukai et al., "Diffusion tensor imaging can detect the early stages of cartilage damage: A comparison study," *BMC Musculoskelet Disord*, vol. 16, pp. 1–7, 2015.
[66] J. Finsterbusch, "B0 Inhomogeneity and Shimming," in *Quantitative MRI of the Spinal Cord*. San Diego, CA, USA: Acad. Press, 2014, Ch. 2.2, pp. 68–90.
[67] J. Tsao, "Ultrafast imaging: Principles, pitfalls, solutions, and applications," *J. Magn. Reson. Imag.*, vol. 32, no. 2, pp. 252–266, 2010.
[68] E. U. Saritas, S. J. Holdsworth, and R. Bammer, "Susceptibility Artifacts," in *Quantitative MRI of the Spinal Cord.* San Diego, CA, USA: Acad. Press, 2014, Ch. 2.3, pp. 91–105.
[69] N. K. Chen and A. M. Wyrwicz, "Correction for EPI distortions using multi-echo gradient-echo imaging," *Magn. Reson. Med.*, vol. 41, no. 6, pp. 1206–1213, 1999.
[70] M. H. In and O. Speck, "Highly accelerated PSF-mapping for EPI distortion correction with improved fidelity," *MAGMA*, vol. 25, no. 3, pp. 183–192, 2012.
[71] X. Hong et al., "Evaluation of EPI distortion correction methods for quantitative MRI of the brain at high magnetic field," *Magn. Reson. Imag.*, vol. 33, no. 9, pp. 1098–1105, 2015.
[72] J. G. Ojemann et al., "Anatomic localization and quantitative analysis of gradient refocused echo-planar FMRI susceptibility artifacts," *Neuroimage*, vol. 6, no. 3, pp. 156–167, 1997.
[73] Y. C. Kim, J. F. Nielsen, and K. S. Nayak, "Automatic correction of echo-planar imaging (EPI) ghosting artifacts in real-time interactive cardiac MRI using sensitivity encoding," *J. Magn. Reson. Imag.*, vol. 27, no. 1, pp. 239–245, 2008.
[74] H. C. Chang and N. K. Chen, "Joint correction of nyquist artifact and minuscule motion-induced aliasing artifact in interleaved diffusion weighted EPI data using a composite two-dimensional phase correction procedure," *Magn. Reson. Imag.*, vol. 34, no. 7, pp. 974–979, 2016.
[75] V. B. Xie et al., "Robust EPI nyquist ghost removal by incorporating phase error correction with sensitivity encoding (pec-sense)," *Magn. Reson. Med.*, vol. 79, no. 2, pp. 943–951, 2018.
[76] J. D. Ianni, E. B. Welch, and W. A. Grissom, "Ghost reduction in echo-planar imaging by joint reconstruction of images and line-to-line delays and phase errors," *Magn. Reson. Med.*, vol. 79, no. 6, pp. 3114–3121, 2018.
[77] A. J. V. Benjamin et al., "Multi-shot echo planar imaging for accelerated cartesian MR fingerprinting: An alternative to conventional spiral MR fingerprinting," *Magn. Reson. Imag.*, vol. 61, pp. 20–32, 2019.
[78] H. Jung et al., "Ye k-t focuss: A general compressed sensing framework for high resolution dynamic MRI," *Magn. Reson. Med.*, vol. 61, no. 1, pp. 103–116, 2009.
[79] O. Afacan et al., "Rapid full-brain FMRI with an accelerated multi shot 3D EPI sequence using both UNFOLD and GRAPPA," *Magn. Reson. Med.*, vol. 67, no. 5, pp. 1266–1274, 2012.
[80] N. Todd et al., "Prospective motion correction of 3D echo-planar imaging data for functional MRI using optical tracking," *Neuroimage*, vol. 113, pp. 1–12, 2015.
[81] T. Liimatainen et al., "MRI contrasts in high rank rotating frames," *Magn. Reson. Med.*, vol. 73, no. 1, pp. 254–262, 2015.